RELATION BETWEEN CORONAL MASS EJECTIONS AND THEIR INTERPLANTARY COUNTERPARTS

N. Gopalswamy

Center for Solar Physics and Space Weather, Department of Physics, The Catholic University of America, Washington DC 20064, USA and NASA Goddard Space Flight Center, Greenbelt, MD 20771, USA

ABSTRACT

Our current knowledge on coronal mass ejections (CMEs) comes from two spatial domains: the near-Sun (up to 30 solar radii) region remote-sensed by coronagraphs and the geospace and beyond where *in situ* observations are made by spacecraft. Comparing observations from these two domains has helped us understand the propagation and evolution of CMEs through the interplanetary (IP) medium and develop an empirical model to predict the 1-AU arrival of CMEs. In this paper, we review the available information on the relation between CMEs and their IP counterparts. In particular, we concentrate on issues related to the prediction of the arrival of ICMEs in the geospace. We discuss the solar sources of the three largest geomagnetic storms of year 2000 and compare the predicted and observed arrival times of the associated CMEs.

1. INTRODUCTION

Coronal Mass ejections (CMEs) are large-scale magnetized plasma structures that erupt from the Sun and are transported in to the heliosphere (Tousey, 1973). They exhibit various observational signatures depending on their age and location of observation in the heliosphere. Billions of tons of material are dumped into the solar wind during each ejection; several CMEs can take place on a single day during the maximum of solar activity cycle. CMEs are multithermal structures in general, carrying coronal (~2 MK) material in the front followed by cool prominence (~8000 K) material in some cases and hot flare-material (~10 MK) in others. When a CME erupts, it leaves behind hot post-eruption arcades or flare loops that mark the location of the eruption on the Sun. CMEs drive powerful interplanetary (IP) shocks, which in turn accelerate electrons and ions over extended periods of time. The accelerated electrons produce type II radio bursts in the IP medium. While the protons and heavier ions accelerated by the shock near the Sun reach 1 AU in a few tens of minutes, the shock arrives carrying locally accelerated energetic storm particles (ESPs).

Spacecraft instruments can directly sample the CMEs. Since CMEs propagate long distances before reaching the spacecraft, they are considerably evolved and hence it is difficult to relate the *in situ* observations to the CME substructures observed near the Sun. The generic term used for CMEs in the solar wind is 'ejecta'. Interplanetary CME (ICME) is another general term used to describe the CME-like disturbance in the solar wind. When the ejecta contains ordered magnetic field it is known as a magnetic cloud (Burlaga *et al.*, 1981). Disordered magnetic fields are also commonly observed in the ejecta (e.g., Hundhausen, 1972); magnetic clouds constitute only a small fraction (~1/3) of the IP ejecta. *In situ* observations of CMEs can be used to infer the magnetic field topology of the IP CMEs (ICMEs) and the physical conditions of their birthplace near the Sun (see, e.g., Henke *et al.*, 1998; Lepri *et al.*, 2001). Most often, the spacecraft in the solar wind detect the following sequence of structures: IP shock, sheath, and ejecta. On rare occasions, one observes cool dense material towards the end of the ejecta that resemble the prominence resting at the bottom of the coronal cavity in the pre-eruption phase of CMEs (Gopalswamy *et al.*, 1998). As a working hypothesis, one can relate CMEs and ICMEs as follows: CME shock → IP shock, CME front → sheath, CME void → ejecta, and CME core → pressure pulse.

CMEs are relevant for two aspects of space weather: 1. Geomagnetic storms and the consequent geoeffects, and 2. solar energetic particles (SEPs and ESPs). When a CME impinges up on the Earth's magnetosphere, it causes geomagnetic storms provided the IP magnetic field carried by it has a southward component. The earliest disturbance that arrives at 1 AU is the shock ahead of the CME, and marks the onset of the storm, usually referred to as "storm sudden commencement" or SSC. However, not all geomagnetic storms are preceded by SSCs. The

shock arrival is also important as they bring the ESPs with them. In this review, we will concentrate on the arrival of CMEs at 1 AU. The arrival of shocks ahead of the CMEs can be inferred from the CME arrival using the standard piston-shock relationship. We also discuss how the speed with which CMEs arrive at 1 AU could be predicted form their initial speed.

2. THE EMPIRICAL CME ARRIVAL MODEL

Availability of simultaneous data on CMEs and ICMEs has made it possible to estimate the influence of solar wind on CMEs as they propagate away from the Sun. Gopalswamy *et al.* (2000a) selected about two dozen IP ejecta observed by the Wind spacecraft and identified the corresponding frontside CME events observed by the Solar and Heliospheric Observatory (SOHO) mission's Large Angle and Spectrometric Coronagraph (LASCO). Assuming that the same object remote-sensed by the coronagraph propagates to the spacecraft in the solar wind, they found that CMEs are subjected to an IP acceleration (a) that depends linearly on the CME initial speed (u): $a = \alpha - \beta u$. Here α and β are positive constants determined from the scatter plot of a and u. The IP acceleration was obtained from the CME speed, ICME speed and the transit time of the CME to 1 AU. The critical speed given by $u_c = \alpha/\beta$ was identified as the solar wind speed. The acceleration was positive $u > u_c$ and negative for $u < u_c$ otherwise, consistent with the observed distribution of CME speeds near the Sun and at 1 AU. Assuming that all the CMEs undergo the same acceleration given above, one can solve the kinematic equation $S = ut + \frac{1}{2} at^2$ to get the time (t) taken by any CME to reach the distance S = 1 AU. The solution t as a function of u is the prediction model.

Gopalswamy *et al.* (2001a) considered two of the limitations of the above empirical model: 1. Projection effects in determining the space speed of Earth-directed CMEs, and 2. the spatial extent over which the IP acceleration operates. To avoid the projection effects, they considered data from remote- and local-sensing spacecraft that had orthogonal views. Helios-1 and the Pioneer Venus Orbiter (PVO) were in quadrature with the P78-1 satellite in the 1970s and 1980s (Sheeley *et al.*, 1985; Lindsay *et al.*, 1999). Limb CMEs detected by Solwind coronagraph on board P78-1 that headed towards either Helios-1 or PVO were identified to get the a versus u relationship, thus minimizing the projection effects. This resulted in α = 2.193 and β = *0.0054*. The constants α and β are adjusted such that the units of a and u are $m.s^{-1}$ and $km.s^{-1}$, respectively. The acceleration cessation distance depends on both the CME speed and the background solar wind speed. Gopalswamy *et al.* (2001a) crudely estimated this distance to be about 0.76 AU. Solving the above kinematic equation for S = 0.76 AU and assuming that the CME propagates freely beyond 0.76 AU, they obtained the prediction curve labeled G in Figure 1. In order to test the validity of this model, they used 47 new events observed by SOHO and Wind (diamond symbols in Figure 1). The prediction agrees with the observation within about 11 hours. While the agreement is very good for the fast CMEs, there is considerable scatter for the low CMEs. In the next subsection, we compare this model with other works related to the prediction of CME arrival.

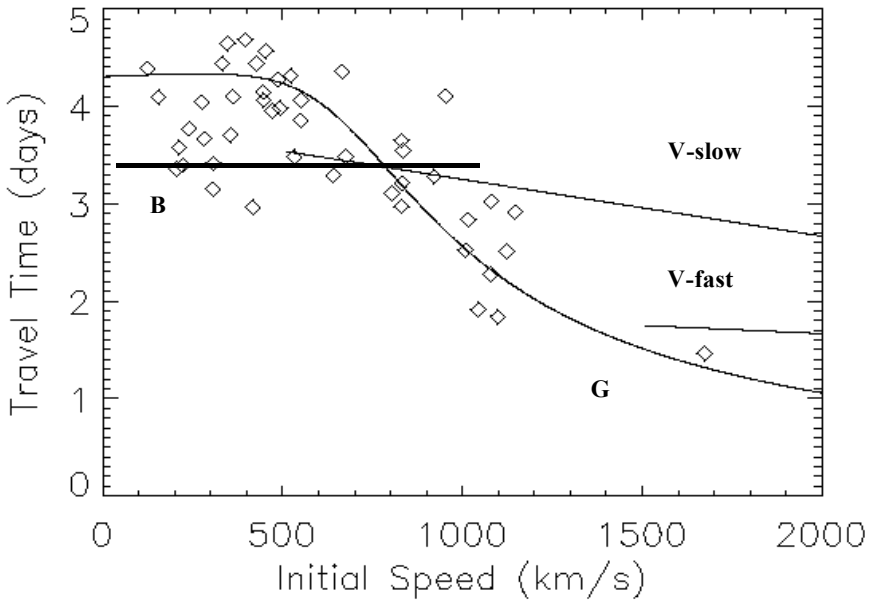

Fig. 1. Travel time of CMEs as a function of their initial speed. The solid curve (G) is the prediction model of Gopalswamy *et al.* (2001a). The two straight lines (V-slow, V-fast) are from Vandas *et al.* (1996) for the propagation of a flux rope through slow and fast background solar winds, respectively. The diamonds represent the measured travel time for a set of 47 events for which CME and ICME observations were available from SOHO and Wind, respectively (see Gopalswamy *et al.*, 2001a for details on these events).

2.1 Comparison with Other Models

Brueckner *et al.* (1998) compared the timings of 8 solar-minimum CMEs observed by LASCO with the onset of geomagnetic storms identified from the Kp index. They concluded that 6 of the events had an average travel time of ~80 hours. The thick solid line (B) in Figure 1 represents this 80-hour rule. The CMEs were either halo or semi-halo events. Clearly some data points lie close to this line, but most of them lie above the line. We did not extend the line beyond 1000 km/s because they have stated that their rule may not apply to higher speed CMEs. It must me pointed out that Brueckner *et al.* (1998) estimated the travel time to be the interval between CME onset at the Sun and the time when Kp reaches its maximum value. The latter is not the same as the CME arrival at 1 AU, but not too different from it.

Vandas *et al.* (1996) performed a parametric study of magnetic cloud propagation with a computational boundary starting at 18 solar radii (Rs) from the Sun. They considered a slow (250 km/s) and a fast (750 km/s) solar wind flows into which the magnetic cloud was injected. They obtained a travel time, which depends linearly on the initial speed of the cloud, as shown in Figure 1 (straight lines marked V-slow and V-fast). The lowest speed of the cloud used in the slow-wind (fast-wind) model was 500 km/s (1500 km/s) so V-fast and V-slow lines have different starting points. Both the fast- and slow-wind models of Vandas *et al.* (1996) predict a travel time much larger than that of Gopalswamy *et al.* (2001a). Note that the Vandas *et al.* curves correspond to a starting distance of 18 Rs, which will slightly increase the propagation time. Their travel-time curves also deviate considerably from the data points.

Recently, Gonzalez-Esparza *et al.* (2002) performed another parametric study, by simulating CME-like disturbances in the solar wind using a one dimensional, hydrodynamic single fluid model. Simulated CMEs were allowed to propagate through a variable ambient solar wind and their 1-AU characteristics were derived. The study showed that the simulated CME pulses suffered a very strong acceleration/deceleration just after their injection against the ambient wind before ~ 0.4 AU and afterwards the magnitude of the acceleration was similar to the interplanetary acceleration proposed by Gopalswamy *et al.* (2000b). The simulation was able to reproduce the general characteristics of the Gopalswamy *et al.* (2001a) prediction model.

2.2 Predicting Final CME Speed

The ICME speed is an important factor in deciding their geoeffectiveness. Therefore, it is useful to predict it from the CME speed measured remotely. The IP acceleration obtained above can be used in another kinematic relation, $v^2 = u^2 + 2aS$ to get the speed of the CME at a distance S. Figure 2 shows the plots of the final speeds obtained for two different values of S. The solid parabolic curve represents the final speed for $S = 0.76$ AU (the distance at which the interplanetary acceleration a is assumed to cease). The dot-dashed parabolic curve represents the final speed for $S = 1$ AU as used in the original work by Gopalswamy *et al.* (2000b). The parabolic curves are not fitted curves to the data points; they are simply the graphic forms of the kinematic equation $v^2 = u^2 + 2aS$, with different values of a and S. We have also plotted two sets of data points in Figure 2: (1) the measured final speeds corresponding to the CME-ICME pairs (diamonds) from archival observations obtained by spacecraft in quadrature, and (2) recent data obtained by SOHO and Wind (crosses). Note that for $u > 600$ km/s, the solid curve fits the data very well. The agreement is not so good for the low-speed events: the predicted speed at 0.76 AU is larger than the observed values. This is expected because the slow CMEs should have stopped accelerating much before reaching 0.76 AU. In fact, we expect a flat profile for all initial speeds less than the solar wind speed, as the observations indicate. We have also plotted two straight lines that relate the final speed to the initial speed based on the method of Lindsay *et al.* (1999). These authors used a scatter plot between the CME speeds (u) and the corresponding ICME speeds (v) and obtained the relation, $v = 0.25u + 360$, where v and u are in units of km/s. The Lindsay *et al.* (1999) relation (dotted straight line) seems reasonable for the low-speed ($u < 500$ km/s) CMEs, but not for the higher speed ones. This line was obtained from a set of 32 CME-ICME pairs collected from Helios-1, PVO, P78-1 and Solar Maximum missions. Gopalswamy *et al.* (2001a) revised this list and came up with a subset of 19 events (diamonds in Figure 2) for which the *in situ* measurements were made at heliocentric distances > 0.7 AU. The dashed straight line is a fit to these 19 data points. We do appreciate the fact that different CMEs stop decelerating at different heliocentric distances, so we expect considerable scatter when predictions are made based on an average cessation distance.

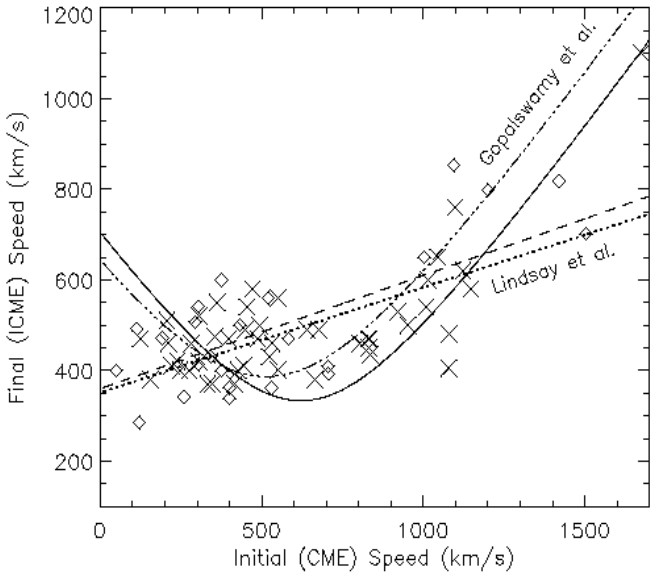

Fig. 2. ICME speed as a function of CME initial speed. The parabolic curves are based on the empirical CME arrival models: dot-dashed curve represents the original model (Gopalswamy *et al.*, 2000) and the solid curve represents the improved model (Gopalswamy *et al.*, 2001a). The dashed line is from Lindsay *et al.* (1999) using a set of 32 events from quadrature observations. The dotted line was obtained in a similar way, but with a subset of 19 events with improved association between CMEs and ICMEs (the diamonds represent this data set). The crosses represent CME-ICME pairs observed recently by SOHO and Wind. The last point corresponds to the fast (1675 km/s) 'Bastille Day' event.

2.3 Comment on Projection effects

When CME speeds were plotted against their source longitudes, Gopalswamy *et al.*, (2000b) found a weak correlation suggesting that disk CMEs are generally of lower speed and that one has to correct for projection effects to obtain the space speed of CMEs. The SOHO-Wind data points used in Figure 2 were not corrected for projection effects, yet Figures 1 and 2 show that predictions based on the initial sky-plane speeds of CMEs are quite reasonable. In fact our attempt to correct the initial speed for projection effects based on the solar-source location of CMEs made the prediction worse. The projection effects depend not only on the source longitude, but also on the cone angle of the CME (see, e.g., Leblanc *et al.*, 2001). Since limb CMEs show a variety of cone angles, one would expect a similar distribution for Earth-directed CMEs. Thus different Earth-directed CMEs are expected to have different widths, so the use of an average width for all the CMEs may not be justified, and might result in a large uncertainty in the correction factor. Another factor to be considered is the variation of the cone angle with time. Gopalswamy *et al.* (2001a) pointed out that the projection effects might partly be compensated for by the initial expansion of the CME. This means the sky-plane speed may not differ from the space speed by a great deal. This does not mean projection effects are unimportant. In fact, the improved estimate of the IP acceleration is a direct result of minimizing projection effects using quadrature observations. The orthogonal viewpoints of the spacecraft in quadrature directly reduce the projection effects, without involving CME widths.

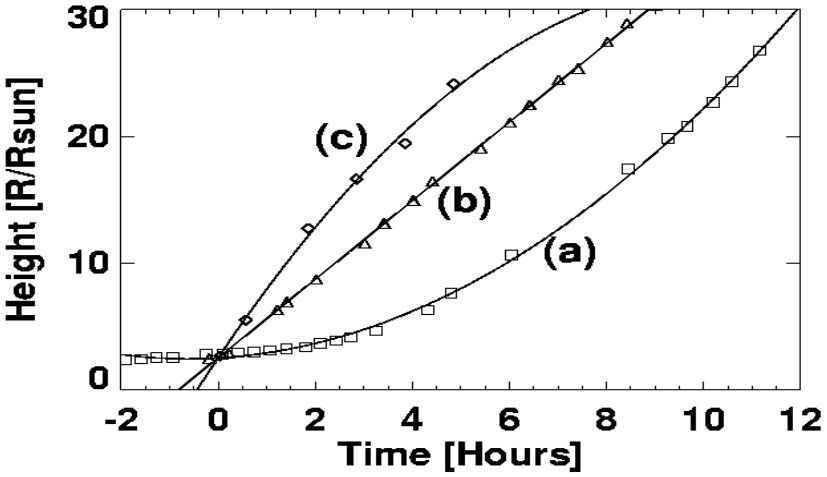

Fig.3. Height-time plots of three representative CMEs observed by SOHO/LASCO. (a) the accelerating CME of June 21, 1998. The propelling forces are most dominant in this case. (b) The constant speed CME of February 17, 2000. In this case, the retarding and propelling forces may balance each other. (c) The decelerating CME of May 11, 1998 where the retarding force seem to be dominant. The plots are normalized to the time the CMEs reach 2.5 Rs.

2.4 Other Effects

In estimating the IP acceleration, we used an average speed obtained from a linear fit to the height-time measurements of the CMEs. In Figure 3 we show three representative height-time plots of CMEs commonly found. Obviously, linear fits will not be appropriate for all the CMEs. When we used quadratic fits, curves (a) and (c) yield positive and negative acceleration, respectively. Plot (c) will result in zero acceleration, and hence linear fit will be appropriate only for such events. Moreover, faster CMEs predominantly decelerate within the coronagraph field of view and the magnitude of the acceleration depends quadratically on the CME speed (Gopalswamy *et al.*, 2001b). The magnitude of the acceleration is generally larger the average IP acceleration. Some slow CMEs may attain higher speeds than what we used because of continued acceleration beyond the coronagraph field of view. This is the likely reason for the slightly earlier arrival of low-speed CMEs than predicted (see Figure 1). Other phenomena which might significantly affect the propagation of CMEs and hence the ability of the prediction model are the CME-CME interactions (Gopalswamy *et al.* 2001c) and the presence of large coronal holes in the vicinity of the eruption region.

2.5 Solar Source

The empirical CME model described above requires the identification of Earth-directed CMEs (Howard et al., 1982). Those CMEs originating closer to the disk center have a better chance of hitting the Earth's magnetosphere. Figure 4 shows the distributions of source longitudes and latitudes of geoeffective during 1996-2000. The bimodal distribution of latitudes simply reflect the location of the sources in the active region belt on either side of the equator. The longitudinal distribution peaks close to the disk center.

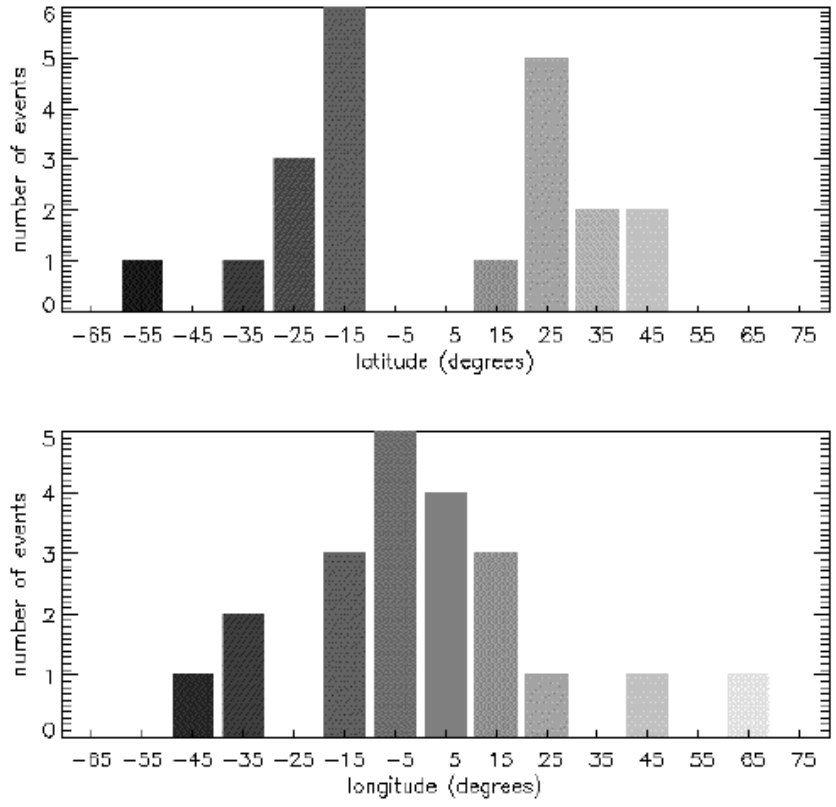

Fig. 4: Latitude (top) and longitude of geoeffective solar CMEs during 1996-2000. Note that most of the CMEs originated from close to the disk center.

Let us consider the largest geomagnetic storms of year 2000 and discuss their solar sources and how they compare with the prediction model. There were three storms with Dst < -200 nT, as listed in Table 1 along with the properties of the associated CMEs. All the three CMEs are halo events. The April 4, 2000 CME resulted in the most intense storm of the year, although the CME was close to the west limb (W66). The storm was of short duration (~1 day) and immediately followed the shock arrival (see Fig. 5a). The LASCO image at 16:43 UT shows that the CME was clearly directed westwards and has the appearance of a central bright structure surrounded by an extended diffuse structure (see Fig. 5b). The latter may be the white-light manifestation of the shock. The ACE spacecraft, which detected the shock at 1 AU must have passed through this shock and its sheath. Iron charge state data indicate a quiet solar wind most of the time except for a short interval roughly coinciding with the duration of the storm (see Fig. 5a). The predicted time of the CME arrival at 1 AU was close to the shock arrival. The "Bastille Day" CME (July 14, 2000) was perfect: it originated from the disk center with very high speed and arrived at 1 AU as predicted by the model (prediction: July 15, 21:00 UT, actual arrival was two hours earlier). The Aug 11, 2000 event was very unusual in that it was relatively slow (~700 km/s) but arrived more than a day ahead of our prediction. Even though it was a western hemisphere event, there

was no solar energetic particle event associated with this CME. The white light CME itself was a perfectly concentric halo CME. When we examined the solar source, we found that it was associated with a C2.3 flare from active region just to the north of the equator. The eruption was accompanied by the disappearance of transequatorial X-ray structures known as coronal dimming. Figure 6 shows two soft X-ray images from Yohkoh/SXT one before and one after the eruption. The X-ray images indicate that there were weak extended coronal holes around the erupting region. The faster wind in the coronal holes might have aided the CME in keeping higher speed so that it reached earlier than expected. Thus, one has to consider not only the properties of the CMEs, but also the environment into which a CME is launched.

Solar Event	**04/04 16:32**	**07/14 10:54**	**08/09 16:30**
Dst	-321 nT	-300 nT	-237 nT
CME speed	1188 km/s	1675 km/s	702 km/s
Solar source	N16 W66	N22 W07	N11 W11
SEP	55 pfu	24000 pfu	None
IP type II	Yes	Yes	No
Shock Arrival	04/06 16:02 UT	07/15 14:02	08/11 18:19 UT
Ejecta Arrival (predicted)	? (04/06 16:30)	07/15 19:00 (21:00)	08/12 06:00 (08/13 09:00)
SW speed	375 km/s	450 km/s	410 km/s
Flare	C 9.7/2F	X5.7/3B	C2.3/SF

Table 1: Solar events associated with the three largest geomagnetic storms of 2000.

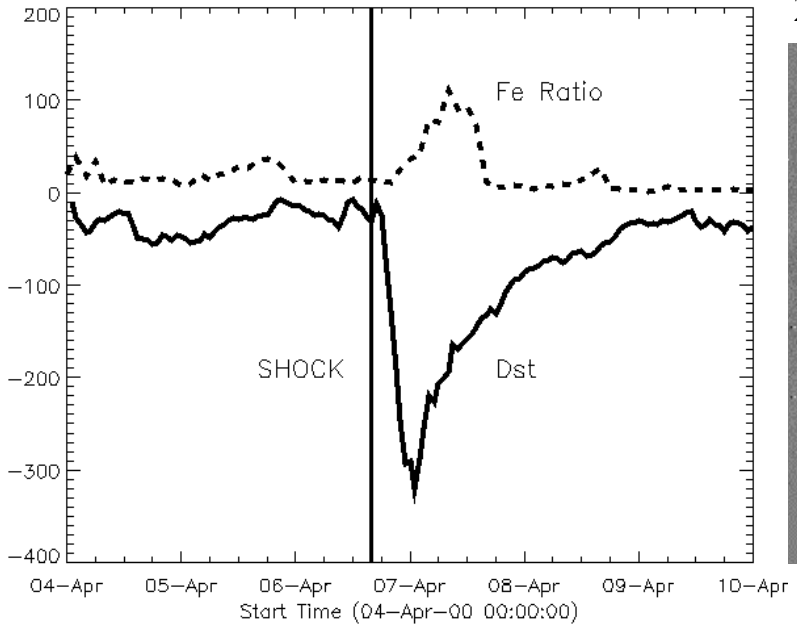

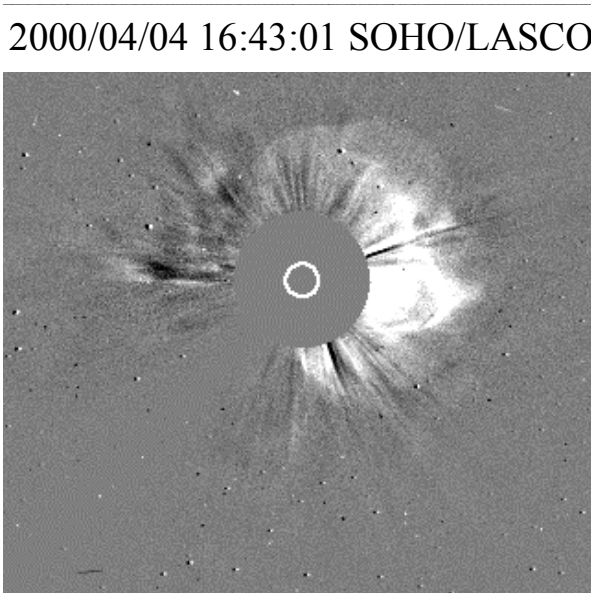

Fig. 5a (left) The geomagnetic storm of April 04, 2000 (as shown by the Dst index) along with the solar wind disturbance represented by the "Fe Ratio," which is the fraction of high-charge state (≥ 16) Fe ion density relative to the total Fe density in all charge states (the ratio was multiplied by a factor of 200 to show on the same plot as the Dst). The thick vertical line around 16 UT on April 16, 2000 represents the IP shock detected *in situ* by ACE (see also Table 1). The elevated Fe ratio behind the shock is the sheath material, which contained a southward magnetic field component and hence resulted in the geomagnetic storm. Fig. 5b (right) SOHO/LASCO C3 difference image showing that the 2000 April 04 event was ejected westward. The solar source was at N16 W66. The CME was geoeffective and produced the most intense geomagnetic storm (-321 nT) in 2000.

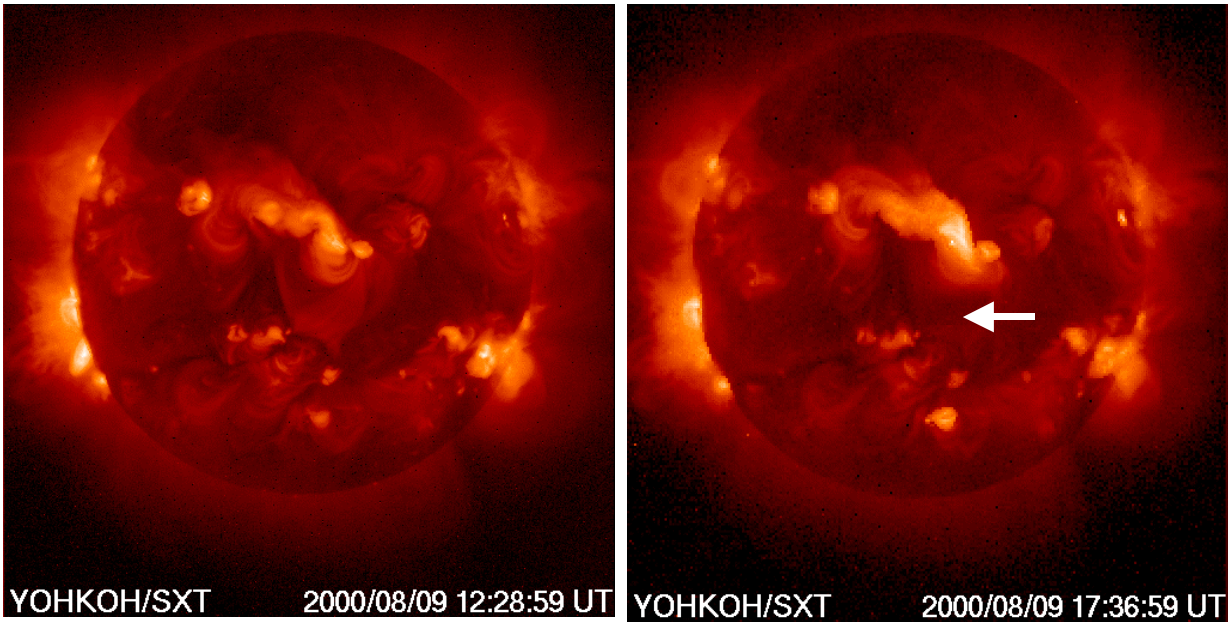

Fig.7: Soft X-ray images from the Yohkoh mission's soft X-ray telescope (SXT) before (left) and after (right) the 2000 August 09 eruption. Some of the transequatorial structures (pointed by the arrow) can be seen missing. The structures in the active region complex are simplified in the post-eruption image.

3. DISCUSSION AND CONCLUSIONS

The primary focus of this review has been the connection between near-Sun and near-Earth relationship between CMEs, especially those aspects relevant to the prediction of CME arrival at 1 AU for space weather purposes. We took the simplest approach of treating the CME as a single body without worrying about the internal structure. This approach has been useful to understand the gross propagation of CMEs through the IP medium. In reality, the internal structure may contribute to the continued propulsion of CMEs (see e.g. Yeh, 1995; Chen, 1997). The constant IP acceleration is a crude approximation to the actual acceleration profile. The primary reason is we have only two measurements of the CME speed one near the Sun and the other near the Earth. The planned STEREO mission will have the capability to track CMEs throughout the Sun-Earth connected space, which will help us create a complete radial profile of the CME acceleration. Space speeds of Earth-directed CMEs can also be measured accurately because of the capability for quadrature observations. Two other capabilities exist at present that use radio observations. The IP scintillation (IPS) of distant radio sources (Tokumaru *et al.*, 2000) observed through CME structures can be used to get the acceleration profiles of CMEs. The IPS signal depends crucially on the presence of enhanced turbulence in the vicinity of CMEs. The current understanding is that such turbulence is associated with the sheath of the CME-driven shock. The IPS observations need to be exploited to get a realistic profile of the IP acceleration. The other capability is the IP type II radio bursts which are due to shocks driven by fast and wide CMEs (Bougeret *et al.*, 1995; Reiner and Kaiser, 1999; Gopalswamy *et al.*, 2001b). Of course tracking the shock is not the same as tracking the CME, but one can always use the piston-shock relationship to connect them. Both these radio techniques are useful mainly for fast CMEs that can drive shocks.

The result that the measured sky-plane speed of geoeffective CMEs is a good representation of the space speed needs further exploration. These CMEs may expand uniformly with a speed comparable to the radial speed. Recall that most of the CMEs that had 1 AU counterparts are halo events, consistent with the idea that these CMEs expand rapidly so they can be detected as halos. We conclude that CMEs accelerate and expand inside 0.7 AU to an extent more than the empirical model supposes.

ACKNOWLEDGMENTS

This work was supported by NASA, Air Force Office of Scientific Research, and NSF.

REFERENCES

Bougeret, J.-L., M. L. Kaiser, P. J. Kellogg, R. Manning, K. Goetz, S. J. Monson, N. Monge, L. Friel, C. A. Meetre, C. Perche, L. Sitruk, and S. Hoang, Waves: The Radio and Plasma Wave Investigation on the Wind Spacecraft, *Space Sci. Rev., 71*, 231, 1995.

Brueckner, G. E. J.-P. Delaboudiniere, R. A. Howard, S. C. Paswaters, O. C. St. Cyr, R. Schwenn, P. Lamy, Llebaraia, G. Simnett, Lonzerotti, L. J., and Aurass, H., Geomagnetic storms caused by coronal mass ejections (CMEs): March 1996 through June 1997, *Geophys. Res. Lett., 25,* 3019, 1998.

Burlaga, L., Sittler, E., Mariani, F., and Schwenn, R., Magnetic loop behind an interplanetary shock – Voyager, Helios, and IMP 8 observations, *J. Geophys. Res., 86,* 6673, 1981.

Chen, J., Coronal Mass Ejections: Causes and Consequences, in Coronal mass ejections, ed. N. Crooker, J A. Joselyn, and J., Feynman, p. 65, 1997.

Gonzalez-Esparza, J. A., A. Lara, E. Perez-Tijerina, and N. Gopalswamy, A numerical study on the acceleration and transit time of coronal mass ejections in the IP medium, *J. Geophys. Res*., submitted, 2002.

Gopalswamy, N., Y. Hanaoka, T. Kosugi, R. P. Lepping, J. T. Steinberg, S. Plunkett, R. A. Howard, B. J. Thompson, J. Gurman, G. Ho, N. Nitta, and H. S. Hudson, On the relationship between coronal mass ejections and magnetic clouds, *Geophys. Res. Lett., 25,* 2485, 1998.

Gopalswamy, N., M. L. Kaiser, B. J. Thompson, L. F. Burlaga, A. Szabo, A. Vourlidas, A. Lara, S. Yashiro, and J. L. Bougeret, Radio-rich Solar Eruptive Events, *Geophys. Res. Lett., 27,* 1427, 2000a.

Gopalswamy, N., A. Lara, R. P. Lepping, M. L. Kaiser, D. Berdichevsky, and O. C. St. Cyr, Interplanetary acceleration of coronal mass ejections, *Geophys. Res. Lett., 27,* 145, 2000b.

Gopalswamy, N., A. Lara, S. Yashiro, M. L. Kaiser, and R. A. Howard, Predicting the 1-AU arrival times of coronal mass ejections , *J. Geophys. Res.,*106, 29,207, 2001b.

Gopalswamy, N., S. Yashiro, M. L. Kaiser, R. A. Howard, and J.-L. Bougeret, Characteristics of coronal mass ejections associated with long-wavelength type II radio bursts , *J. Geophys. Res.,* 106, 29,219, 2001a.

Gopalswamy, N., S. Yashiro, M. L. Kaiser, R. A. Howard, and J.-L. Bougeret, ., *Astrophys. J.,* 548, L91, 2001c.

Henke, T., J. Woch , U. Mall, S. Livi, B. Wilken, *et al.*, Differences in the O^{7+}/O^{6+} ratio of magnetic cloud and non-cloud coronal mass ejections, *Geophys. Res. Lett.,* 25, 3465, 1998.

Howard, R. A., Michels, D. J., Sheeley, N. R., Jr., and Koomen, M. J., The observations of a coronal transient directed at Earth, *Astrophys. J., 263,* L101, 1982.

Hundhausen, A. J., Coronal Expansion and Solar Wind, Springer-Verlag, New York, 1972.

Leblanc, Y., G. A. Dulk, A. Vourlidas, J.-L. Bougeret, Tracing shock waves from the corona to 1 AU: Type II radio emission and relationship with CMEs *J. Geophys. Res., 106,* 2001.

Lepri, S., T. Zurbuchen, L. Fisk, I. Richardson, H. Cane and G. Gloeckler, "Iron charge distribution as an identifier of interplanetary coronal mass ejections, *J. Geophys. Res.,*106, 29231, 2001.

Lindsay, G. M., Luhmann, J. G., Russell, C. T., and Gosling, J. T., Relationships between coronal mass ejection speeds from coronagraph images and interplanetary characteristics of associated interplanetary coronal mass ejections, *J. Geophys. Res.,* 104, 12515, 1999.

Reames, D. V., Particle acceleration at the Sun and in the heliosphere, *Space Sci. Rev.,* 90, 413, 1999.

Reiner, M. J. and M. L. Kaiser, High-frequency type II radio emissions associated with shocks driven by coronal mass ejections, *J. Geophys. Res,*104, 16,979, 1999.

Sheeley, N. R., Jr., R. A. Howard, M. J. Koomen, D. J. Michels, R. Schwenn, K. H. Mulhauser, and H. Rosenbauser, Coronal mass ejections and interplanetary shocks, *J. Geophys. Res*., 90, 163, 1985.

Tokumaru, M., M. Kojima, K. Fujiki, A. Yokobe, Three-dimensional propagation of interplanetary disturbances detected with radio scintillation measurements at 327 MHz, *J. Geophys. Res.,*105, 10435, 2000.

Tousey, R., The solar corona, *Space Res., 13,* 713, 1973.

Tylka, A., New insights on solar energetic particles from Wind and ACE, *J. Geophys. Res.,* 106, 25,233, 2001.

Vandas, M., S. Fischer, M. Dryer, Z. Smith, and T. Detman, Parametric study of loop-like magnetic cloud propagation, *J. Geophys. Res.,* 101, 16,545, 1996.

Webb, D. F., E. W. Cliver, N. U. Crooker, O. C. St. Cyr, and B. J. Thompson, *J. Geophys. Res., 105,* 7491, 2000.

Yeh, T, A dynamical model of magnetic clouds, *Asrophys. J.,* 438, 975, 1995.